

X- and γ -Rays Computerized Minitomograph Scanner for Soil Science

PAULO ESTEVÃO CRUVINEL, ROBERTO CESAREO, SILVIO CRESTANA, AND SÉRGIO MASCARENHAS

Abstract—A computerized tomograph scanner system using X- and γ -rays has been developed for applications in soil science. Previous results were obtained using a miniature X-ray tomograph scanner designed for biomedical analysis [1].

As a new methodology of instrumentation and in soil research [2], this apparatus has proven to be useful for measuring volumetric water content θ to an accuracy of $\pm 3\%$ and soil bulk density $\rho \pm 2\%$ (in grams/centimeters³).

The system features translation and rotation scanning modes, a 200-mm effective field of view, signal processing by pulse counting and 1.0-mm spatial resolution. The performance of the system has been demonstrated by experimentally measuring water content and the bulk density of soil samples.

I. INTRODUCTION

TRANSMISSION and emission tomography are widely recognized in medicine as methods of obtaining information about body structure and physiological function.

In a transmission computed tomography (CT) scan, a number of profiles of narrow-beam transmission are made at different orientations to the subject. A cross-sectional reconstruction is generated from these measurements for subsequent analysis. Computerized tomography, as a new method for investigation in soil science physics, has been introduced in [3]–[5]. It has proven to be of great advantage when compared to other classical methods such as gravimetry [6] or γ -ray direct transmission [7]. However, medical CT-scanners are very costly and do not provide sufficient energy output range for studies of soil and plant systems.

This paper describes a compact low-cost (approximately US\$ 50 000) CT-scanner (minitomograph) designed for soil science.

In comparison with classical methods such as direct γ -ray transmission or gravimetric tests, the minitomograph has the following advantages.

- 1) It is possible to measure local heterogeneities within the soil at pixel resolution.

Manuscript received March 30, 1990; revised May 30, 1990. This work was supported by EMBRAPA-UAPDIA, São Carlos, Brazil, and by the ICTP Programme for Training and Research in Italian Laboratories, Trieste, Italy.

P. E. Cruvinel, S. Crestana, and S. Mascarenhas are with Ministério Da Agricultura, EMBRAPA/UAPDIA, S. Carlos/SP, 13560 Brazil, 13560.

R. Cesareo is with the Università Delgi Studi Di Roma, Centro per L'Ingegneria Biomédica, Rome, Italy, 00186.

IEEE Log Number 9037906.

- 2) It is possible to measure soil bulk density and water content pixel by pixel.
- 3) It is possible to non-invasively obtain two- and three-dimensional images of soil samples independent of the geometry and shape of each sample.
- 4) It is possible to use several different beam energies and radioactive sources as well as X-ray fluorescent targets [8].

Two- and three-dimensional measurement of soil physical parameters such as bulk density and water content is an important task in modeling and analyzing soil science problems. There is a need for nondestructive experimental techniques having millimeter or submillimeter resolution capable of investigating the intricacies present in the variety of processes that occur in soils. Some examples of coupled and time dependent soil processes are compaction, root penetration, crusting, seedling cracking and swelling, wetting/drying or thawing/freezing cycles, miscible and immiscible displacement of nutrients in the presence of roots, and preferential flow of pollutants in fractured porous media. X- and γ -rays computerized tomography is becoming a powerful and exciting tool for studying such soil phenomena [9], [10].

II. THE TOMOGRAPHIC METHOD AND PHYSICAL CONSIDERATIONS

A. Principles of the Tomographic Method

Let $f(x, y)$ be a two-dimensional cross-sectional image of a three-dimensional object. The image reconstruction theorem states that $f(x, y)$ can be reconstructed from many one-dimensional measurements (which when plotted are termed projections) made in the x, y plane.

The image reconstruction theorem can be described mathematically with the help of the Fourier transform. Thus if $f(x, y)$ represents a two-dimensional image to be reconstructed in the (x, y) spatial domain it can be transformed to the frequency domain (u, v) , and if $F(u, v)$ is given $f(x, y)$ can be obtained by using the inverse Fourier transform:

$$f(x, y) = \int_{-\infty}^{\infty} \int_{-\infty}^{\infty} F(u, v) \cdot \exp [i 2\pi(ux + vy)] du dv. \quad (1)$$

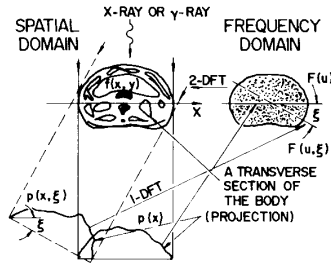


Fig. 1. The principle of Fourier projection theorem used for image reconstruction from projections.

Fig. 1 shows the principle of image reconstruction from projections [11]. Let $p(x)$ be the one-dimensional experimentally measured zero degree projection of $y = p(x)$ onto the x axis. It is then possible to demonstrate that the one-dimensional Fourier transform (1-DFT) of a one-dimensional projection of a two-dimensional image is identical to the corresponding central section of the two-dimensional Fourier transform (2-DFT) of the object. If 30 projections at 6 deg. increments are accumulated and their 1-DFT's are performed, then each of these 30 one-dimensional Fourier transformed projections would represent a corresponding central line of the 2-DFT's of the X-ray or γ -ray cross-sectional image. The collection of all these transformed projections is the 2-DFT of $f(x, y)$.

There are other methods that can also be used to reconstruct a two-dimensional image from its projections. Each different reconstruction method will give a slightly different version of the original image.

The filtered back-projection method, known as the convolution method, is widely used as a reconstruction tool because of its speed, accuracy, and versatility. A polar coordinate system is used and the projection is represented by the integral of the product of the image and the delta function. Fig. 2 shows one projection $m(t, \xi)$ of the object at angle ξ and displacement t

$$m(t, \xi) = \int_0^{2\pi} \int_0^{\infty} f(l, \xi') \cdot \delta[t - l \cos(\xi - \xi')] l dl d\xi' \quad (2)$$

where $f(l, \xi')$ is the pixel value of the object at (l, ξ') and δ is the delta function. From the shifting property of the delta function, the 1-DFT of $m(t, \xi)$, $M(\Omega, \xi)$, is

$$M(\Omega, \xi) = \int_0^{2\pi} \int_0^{\infty} f(l, \xi') \cdot \exp[-i2\pi\Omega l \cos(\xi - \xi')] l dl d\xi'. \quad (3)$$

The 2-DFT of $f(l, \xi)$, $F(\Omega, \xi)$ is given by

$$F(\Omega, \xi) = \int_0^{2\pi} \int_0^{\infty} f(l, \xi') \exp[-i2\pi\Omega l \cdot \cos(\xi - \xi')] l dl d\xi'. \quad (4)$$

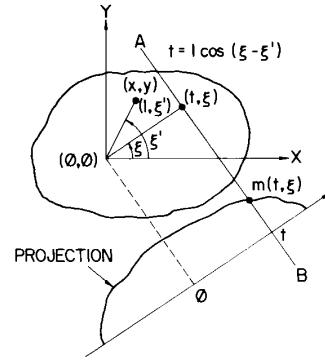


Fig. 2. One projection of the object at angle ξ , $m(t, \xi)$.

Comparing (3) and (4), it is found that $M(\Omega, \xi) = F(\Omega, \xi)$.

The 1-DFT of the projections of an object at angle ξ is the central section at the same angle ξ of the 2-DFT of the object. This is the central slice theorem [12]. In order to completely reconstruct the object in continuous space, an infinite number of projections are required to fill the whole Fourier space.

Let $G(\Omega, \xi) = |\Omega| M(\Omega, \xi)$, it is then possible to obtain

$$g(t, \xi) = \int_{-\infty}^{\infty} |\Omega| M(\Omega, \xi) \exp(i2\pi\Omega t) d\Omega \quad (5)$$

where $t = x \cos \xi + y \sin \xi$ and $g(t, \xi)$ is the inverse Fourier transform of $G(\Omega, \xi)$. The convolution theorem states that the Fourier transform of two multiplicative functions is equal to the convolution of the transform of the function

$$g(t, \xi) = h(t) * m(t, \xi) \quad (6)$$

where $h(t) = \int_{-\infty}^{\infty} |\Omega| \exp(i2\pi\Omega t) d\Omega$, is the inverse Fourier transform of $|\Omega|$, and

$$h(t) * m(t, \xi) = \int_{-\infty}^{\infty} h(t - \tau) m(\tau, \xi) d\tau \quad (7)$$

is the convolution integral.

The inverse Fourier transform of $|\Omega|$, which is $h(t)$, means that for any point (x, y) in the object, the reconstruction is the summation of $g(t, \xi)$ for all ξ , which is exactly the same as the filtered $[h(t)]$ back-projection $[m(t, \xi)]$. The procedure of reconstruction is thus the back-projection of the convolution of the projection and the filter, thus

$$f(x, y) = \int_0^{2\pi} h(t) * m(t, \xi) d\xi. \quad (8)$$

In the present paper, the images have been reconstructed by using the filtered back-projection algorithm with a Ram-Lak filter [13].

B. Physical Considerations

Linear attenuation coefficients are convenient for engineering applications, they are proportional to the attenuation density, ρ , which depends on the physical state of the material.

A narrow beam of monoenergetic photons with energy E and incident photon flux density I_0 on passing through a non-homogeneous absorber of thickness x , will have an emerging photon intensity I given by

$$I = I_0 \exp \left(\oint_s \left\{ \left[\frac{\mu(Z, E)}{\rho} \right] \rho x \right\} ds \right) \quad (9)$$

where s is any direction across the absorber and μ is the linear attenuation coefficient (in units of length^{-1}) for material of physical density ρ , atomic number Z and μ/ρ is the mass attenuation coefficient.

Even though one can identify an approximate proportionality of ρ to the atomic number Z for a given physical state, the error in this approximation can for certain materials exceed the typical resolution capabilities of CT-scanners.

If the absorber is a chemical compound or mixture, its mass attenuation coefficient μ/ρ can be approximately evaluated from the coefficients for its constituent elements according to the sum

$$\frac{\mu}{\rho} = \sum_i w_i \frac{\mu_i}{\rho_i} \quad (10)$$

where w_i is the proportion by weight of the i th constituent.

The mass attenuation coefficient μ/ρ is also proportional to the total photon interaction cross section per atom, σ_{tot}^a ; that is, the sum of the cross sections for all the elementary scattering and absorption processes. The appropriate relation is

$$(\mu/\rho)[\text{cm}^2/\text{g}] = \sigma_{\text{tot}}^a[\text{cm}^2/\text{atom}] \cdot (N/A)[\text{atoms}/\text{g}] \quad (11)$$

where N is Avogadro's number and A is the atomic mass of the absorber.

Therefore, the total mass attenuation coefficient μ/ρ can be decomposed into contributions from each mode of photon interaction as

$$\mu/\rho = \mu R/\rho + \mu F/\rho + \mu C/\rho \quad (12)$$

where R , F , and C designate Rayleigh scattering, photoelectric effect, and Compton scattering, respectively.

The electronic cross section, σ_{tot}^e , is also the sum of contributions from those of the individual photon interaction mechanisms

$$\sigma_{\text{tot}}^e = \sigma_R^e + \sigma_F^e + \sigma_C^e. \quad (13)$$

The terms on the right-hand side of (13) explicitly determine the energy and atomic composition dependence of μ .

Equations (11)–(13) combine to yield

$$\mu/\rho = \frac{NZ}{A} (\sigma_R^e + \sigma_F^e + \sigma_C^e). \quad (14)$$

The CT-scanner obtains a map of the linear attenuation coefficients for X- or γ -rays in the scanned section of the sample. For biological objects, at the energy values usually employed in CT-scanners (70–80 keV mean energy) attenuation coefficients are mostly due to the Compton effect, which is proportional to the electronic density (μ/ρ) of the materials. Except for hydrogen, the electronic density is with good approximation proportional to the physical density.

The situation is not different for analyzing soil samples. For soils the contribution of the Compton effect is approximately 80% at 80 keV, the remaining contribution is mainly due to the photoelectric effect. Therefore, a tomographic map of soil at 60–100 keV is to a first approximation proportional to the distribution of the physical density, while a tomographic map at lower energy (20–30 keV) would be mainly proportional to a power of the atomic number Z , and the photoelectric effect would be dominant.

III. SYSTEM DESIGN

Fig. 3 shows the block diagram of the system configuration. The hardware comprises a mechanical table with two stepper motors (one for rotation and one for translation), a radiation source, collimators, a scintillator detector (NaI(Tl) crystal), an electronic pulse counting and processing system, a microcomputer, a high resolution video monitor and a graphic printer. We have used an 8-b microcomputer based on a Motorola 6502 microprocessor.

The scanning mechanism of the minitomograph consists of an X-ray tube (60 kVp, 60 mA) or a γ -ray radioactive source (^{241}Am , 60 keV, 300 mCi), a detector system and two stepper motors which control the relative position of the tomographic table. The stepper motors control cards have been designed as a four-phase motor drive that needs a clock or microprocessor pulse to determine the stepping rate, which is 180 steps per second. The accuracy of each 1.8° step angle is 2.5%. This error is noncumulative and averages to zero in 360° . The controls for the rotation and translation of the tomographic table have been designed using stepper motors. Fig. 4 shows the schematic diagram and the time sequence of the stepper motor controls. These signals are generated to operate the stepper motors and to control the rotation sense.

Optoelectronic devices and comparator circuits were used to define and initialize coordinate positions of the tomographic table. Fig. 5 shows the schematic diagram and the time sequence of the tomographic table position controls.

The interface has been designed using two Motorola 6821 peripheral interface adapter integrated circuits. These I/O ports are used to interface the stepper motors control cards, the control cards for the tomographic table

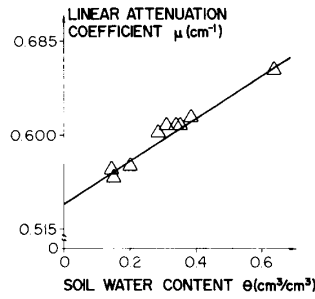


Fig. 7. $\mu (\text{cm}^{-1}) = (0.415 \pm 0.009) + (0.254 \pm 0.008) \theta (\text{cm}^3/\text{cm}^3)$; Calibration curve $\mu (\text{cm}^{-1})$ versus soil water content in $\theta (\text{cm}^3/\text{cm}^3)$ at incident energy of 60 keV ($r^2 = 0.970$).

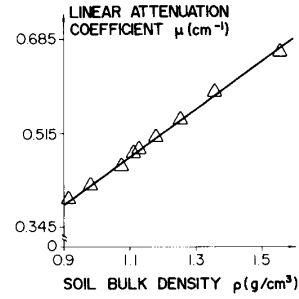


Fig. 8. $\mu (\text{cm}^{-1}) = (0.006 \pm 0.010) + (0.426 \pm 0.009) \rho (\text{g}/\text{cm}^3)$; Calibration curve $\mu (\text{cm}^{-1})$ versus soil bulk density in $\rho (\text{g}/\text{cm}^3)$ at incident energy of 60 keV ($r^2 = 0.997$).

statistical fluctuation error was lower than 1.5% because the number of detected photons was larger than 10^4 .

Tomographs have been measured for samples with different mean values of water content and the results are reported in Fig. 7. For the non-swelling soil employed, there is a very good linear relationship between the linear attenuation coefficient and the water content of the soil (coefficient of linear correlation $r^2 = 0.970$):

$$\mu (\text{cm}^{-1}) = (0.415 \pm 0.009) + (0.254 \pm 0.008) \theta (\text{cm}^3/\text{cm}^3).$$

A set of soil bulk density values have been measured at 60 keV for air dried soil samples of non-swelling latosol. Results are reported in Fig. 8.

Once again there is a very good linear relationship between linear attenuation coefficient and the soil bulk density (coefficient of linear correlation $r^2 = 0.997$):

$$\mu (\text{cm}^{-1}) = - (0.006 \pm 0.010) + (0.426 \pm 0.009) \rho (\text{g}/\text{cm}^3).$$

The attenuation cross section of soil employed in this experiment was $0.433 \text{ cm}^2/\text{g}$ and from the above equation the mass attenuation coefficient versus density is constant, within the experimental error, showing the prevalent contribution of the Compton effect at 60 keV.

In these experiments the minimum acquisition time for a tomograph with the present apparatus is about 20 min.

For quality evaluation (quantitative analysis) of the images the contrast transfer function (CTF) method of analysis has been used [15]. In this method, the CTF is plotted versus the spatial frequency. The CTF for a spatial frequency is given by the relative amplitude of the oscillations observed in the attenuation profile that passes through the set of holes. The test object was a 30-mm diameter plexiglass disk having three sets of two holes of various sizes. The diameters of the holes were 1.0, 3.0, and 6.0 mm. Therefore, to obtain an indication of the contrast resolution the standard deviation (σ) from the mean attenuation was calculated for 30×30 pixels occupying a region of the image. Fig. 9 shows an image reconstructed on pixels with widths of 1.0 mm and an attenuation profile $\mu (\text{cm}^{-1})$ versus distance $d (\text{cm})$ from

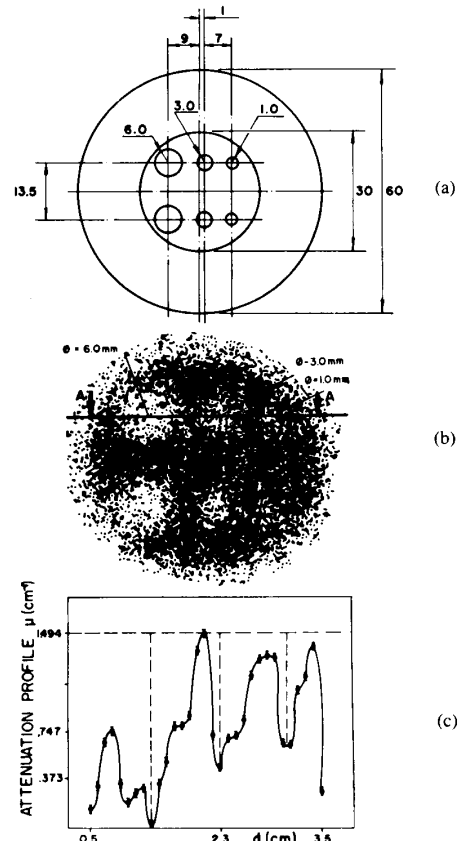


Fig. 9. (a) The test object. (b) An image reconstructed on pixel with width of 1.0 mm. (c) An attenuation profile $\mu (\text{cm}^{-1})$ versus distance $d (\text{cm})$. The profile relates to line A-A.

the test object. A loss of spatial resolution at a pixel width of 2.0 mm has been confirmed by the CTF shown in Fig. 10. On the other hand, the spatial resolution was not improved by decreasing the pixel width to 0.5 mm.

V. CONCLUSIONS

The main results obtained are listed as follows.

- i) The calibration curve (Fig. 7) of linear attenuation coefficient $\mu (\text{cm}^{-1})$ versus the volumetric water

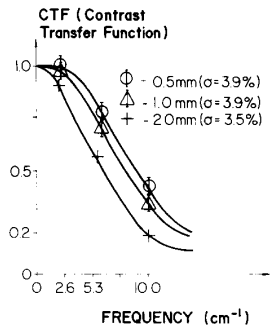


Fig. 10. CTF and relative standard deviation, σ , for pixel widths of 0.5, 1.0, and 2.0 mm.

content of the soil θ (cm^3/cm^3) at 60 keV and $r^2 = 0.970$ shows the minitomograph capability for measuring soil water content.

- ii) The calibration curve (Fig. 8) of linear attenuation coefficient μ (cm^{-1}) versus the soil bulk density ρ (g/cm^3) at 60 keV and $r^2 = 0.997$ shows the minitomograph capability for measuring the soil bulk density.
- iii) The standard deviation from the mean attenuation did not change significantly with the beam width, however, the counting time was adjusted so that an equal number of photons contributed to each image. For the images generated with the minitomograph system, the best spatial resolution was obtained with a pixel width of 1.0 mm.

ACKNOWLEDGMENT

The authors wish to thank Ana Maria Felicori Ambrosio for the secretarial help.

REFERENCES

- [1] R. Cesareo and L. M. F. Storelli, "A miniature X-ray tomography scanner employing radioisotopic sources," presented at the Int. Conf. on Appl. Physics to Medicine and Biology, Trieste, Italy, Mar. 30-Apr. 3, 1982.
- [2] S. Crestana, R. Cesareo, and S. Mascarenhas, "Using a computed tomography miniscanner in soil science," *Soil Sci.*, vol. 142, pp. 56-61, 1986.
- [3] A. M. Petrovic, J. E. Siebert, and P. F. Riede, "Soil bulk density analysis in three dimensions by computed tomographic scanning," *Soil Sci. Soc. Amer. J.*, vol. 46, pp. 445-450, 1982.
- [4] J. M. Hainsworth and I. A. G. Aylmores, "The use of computer assisted tomography to determine spatial distribution of soil water content," *Aust. J. Soil Res.*, vol. 21, pp. 435-443, 1983.
- [5] S. Crestana, S. Mascarenhas, and R. S. Pozzi-Mucelli, "Static and dynamic three-dimensional studies of water in soil using computed tomographic scanning," *Soil Sci.*, vol. 140, pp. 326-332, 1984.
- [6] G. O. Schwab and R. K. Frevert, *Elementary soil and water engineering*. New York: Wiley, pp. 350, 1985.
- [7] C. M. Davisson and R. D. Evans, "Gamma-ray absorption coefficients," *Rev. Mod. Phys.*, vol. 24, pp. 79-106, 1952.
- [8] R. Cesareo, Ed. *X-ray Fluorescence (XRF and PIXE) in Medicine*, Rome, Italy: Acta Medica, p. 239, 1982.
- [9] S. Crestana, S. Mascarenhas, R. Cesareo, and P. E. Cruvinel, "Soil research opportunities using X- and γ - ray computed tomography techniques," presented at the Int. Conf. and Workshop on the Validation of Flow and Transport Models for the Unsaturated Zone, Ruidoso, NM, May 22-25, 1988.
- [10] C. M. P. Vaz, S. Crestana, S. Mascarenhas, P. E. Cruvinel, K. Reichardt, and R. Stolf, "Using a computed tomography miniscanner for studying tillage induced soil compaction," *Soil Technol.*, vol. 2, pp. 313-321, 1989.
- [11] A. M. Cormack, "Nobel award address: Early two-dimensional reconstruction," *Med. Phys.*, vol. 7, 1980.
- [12] R. N. Bracewell, *The Fourier Transform and Its Applications*, 2nd ed. New York: McGraw-Hill, 1986.
- [13] G. N. Ramachandran and A. V. Lakshminarayanan, "Three dimensional reconstruction from radiographic and electron micrographic application of convolutions instead of Fourier transforms," *Proc. Natl. Acad. Sci.*, vol. 68, pp. 2236-2240, 1971.
- [14] D. Hillel, "Soil and water: Physical principles and process," New York: Academic Press, 1971, pp. 365.
- [15] T. Taylor and R. Lupton, "Resolution, artefacts, and the design of computed tomography systems. VIII. Tomography," *Nucl. Instr. Meth. Phys. Res.*, vol. A 242, pp. 603-609, 1986.